THE ASTROPHYSICAL JOURNAL, 487:L155–L159, 1997 October 1

THE BOOMERANG NEBULA: THE COLDEST REGION OF THE UNIVERSE?

RAGHVENDRA SAHAI
Jet Propulsion Laboratory, MS 183-900, California Institute of Technology, Pasadena, CA 91109
AND
LARS-ÅKE NYMAN
European Southern Observatory, Santiago 19, Chile; and Onsala Space Observatory, S-43992 Onsala, Sweden
Received 1997 June 3; accepted 1997 July 17; published 1997 September 2

ABSTRACT

We have discovered absorption of the 3 K microwave background radiation by ultracold CO gas in the Boomerang Nebula, a bipolar reflection nebula illuminated by a star that has recently evolved off the asymptotic giant branch (AGB). During the AGB phase, stars with main-sequence masses of 1–8 $M_\odot$ eject large amounts of matter, affecting their subsequent evolution as well as the chemical and dynamical evolution of the Galaxy. Our new observations of CO and ^{13}CO millimeter-wave lines toward the Boomerang Nebula show it to be quite extreme and perhaps unique in its mass-ejection properties. We find that it has been losing mass through a fast (164 km s^{-1}) molecular wind at a prodigious rate of 10^{-3} $M_\odot$ yr^{-1} (a factor of about 10 larger than the highest rates seen in AGB/post-AGB objects until now) for at least approximately 1500 yr. This wind contains ultracold gas at temperatures below the microwave background temperature, making the Boomerang Nebula the coldest place in the universe found so far (excluding laboratories), and confirming an earlier prediction of the existence of such envelopes. The ^{12}C/^{13}C ratio is rather low (5), close to the lowest value attainable (3) through equilibrium CNO-cycle nucleosynthesis. The mechanical wind momentum ($dM/dt \times V_{\rm exp}$) in the Boomerang Nebula exceeds the total radiative momentum (L_*/c) by a factor greater than 10^4. The data also show the presence of an inner shell, expanding at 35 km s^{-1}, which may have resulted from the ejection of a common envelope by a central binary star.

Subject headings: circumstellar matter — cosmic microwave background — reflection nebulae — stars: AGB and post-AGB — stars: individual (Boomerang Nebula) — stars: mass loss

1. INTRODUCTION

The transition of asymptotic giant branch (AGB) stars into planetary nebulae occurs over a very short period (~1000 yr; see, e.g., Schönberner 1990). Objects in this evolutionary phase, called proto–planetary nebulae (PPNs), are therefore rare objects. Consequently, the protoplanetary phase of stellar evolution is very poorly understood but probably holds the key to the long-standing puzzle of how red giant stars and their surrounding mass-loss envelopes (which are largely round) transform themselves into the dazzling variety of asymmetric morphologies seen in planetary nebulae (e.g., Schwarz, Corradi, & Melnick 1992). The Boomerang Nebula (e.g., Wegner & Glass 1979; Taylor & Scarrot 1980), with its distinctly bipolar morphology similar to that of the prototype PPN, CRL 2688 (e.g., Latter et al. 1993), is an important member of the class of known PPNs. In such nebulae, the central star is hidden behind a dusty, flattened cocoon seen roughly edge-on, allowing starlight to escape preferentially along the polar directions and to illuminate a pair of reflection nebulosities above and below the cocoon. Almost all of the nebular material surrounding the obscured central star in PPNs consists of cold molecular gas, ideally probed through observations of millimeter-wave rotational lines. In this Letter, we report such observations of the Boomerang Nebula, which show it to be a unique object, consisting of an ultracold and extremely massive molecular envelope, expanding at a very high speed. The extreme physical characteristics of the Boomerang Nebula reported here have never been seen before in any AGB or post-AGB object and should spur new theoretical and observational efforts to understand the nature of the mass-loss processes occurring during late stellar evolution.

2. OBSERVATIONS AND RESULTS

Millimeter-wave CO observations of the Boomerang Nebula were made using the 15 m SEST (Swedish ESO Submillimeter Telescope), situated on La Silla, Chile. The data were obtained during 1995 (August to October) and 1994 August, using SIS receivers at 3 and 1.3 mm. The beamwidths of the telescope at the CO $J = 1$–0 and 2–1 frequencies (115 and 230 GHz) are 45″ and 24″, respectively. Acousto-optical spectrometers with bandwidths of 1 and 0.5 GHz were used to record the 1–0 and 2–1 spectra. The channel separation was 0.7 MHz, and the resolution was 1.4 MHz. All intensities are given in $T_{\rm mb}$, which is the chopper wheel corrected antenna temperature, T_A^*, divided by the main-beam efficiency (0.7 for 1–0 and 0.6 for 2–1). Pointing was checked on a nearby SiO maser and is estimated to be accurate to better than 3″ rms. The telescope was used in a dual beam switch mode with the source alternately placed in each of the two beams, a method that yields very flat baselines and a reliable continuum level. The beam separation was about 11′.5.

The ^{12}CO and ^{13}CO (1–0) spectra (Fig. 1) both show a very broad absorption feature. The absorption is not artificially produced by emission in the OFF position, because spectra taken by position switching against several OFF positions at different distances from the object (up to several degrees) always produced the same absorption feature. Bujarrabal & Bachiller (1991, hereafter BB) had previously observed CO lines in the Boomerang Nebula, but they reported only the central emission feature. At that time, however, Schottky receivers were used, which produced 2–3 times more noise than the present system and poor baselines over a shorter bandwidth (500 MHz, compared to the present 1 GHz), making it difficult to detect wide and weak absorption features. The LSR radial velocity of the

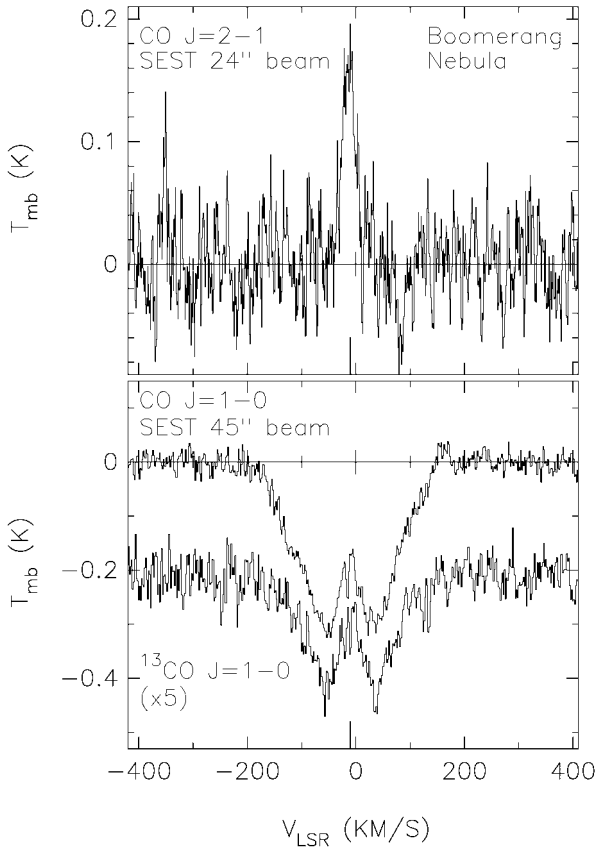

FIG. 1.—CO (1–0), ^{13}CO (1–0), and CO (2–1) spectra taken toward the center of the Boomerang Nebula ($\alpha_{1950} = 12^h41^m54\overset{s}{.}2$, $\delta_{1950} = -54°14'47''$) using the 15 m Swedish ESO Submillimetre Telescope. The ^{13}CO (1–0) spectrum has been scaled by a factor of 5, and a constant (0.2 K) has been subtracted to shift it away from the CO (1–0) spectrum for clarity. The LSR radial velocity of the central star (-10 km s^{-1}), measured from the center of symmetry of the CO $J = 2$–1 line, is marked in the spectra. The negative temperatures seen in the $J = 1$–0 spectra result from absorption of the microwave background radiation by ultracold gas in the nebula.

central star (-10 km s^{-1}), measured from the center of symmetry of the CO $J = 2$–1 line, is marked in the spectra.

The broad absorption feature in the ^{12}CO and ^{13}CO (1–0) spectra implies an unusually large outflow velocity ($V_{exp} = 164$ km s^{-1}). Similarly high outflow velocities have also been noted from absorption lines seen in optical spectra of the nebula (Neckel et al. 1987). The central emission feature in the spectra indicate a second outflow with a smaller expansion velocity (35 km s^{-1}). In the CO $J = 2$–1 transition, only the central emission feature is seen—there are no absorption features. We have also mapped the nebula in the CO $J = 1$–0 transition in order to determine its spatial structure and extent. Maps of the CO (1–0) features in different velocity intervals show that the distribution of molecular gas in the nebula is largely roughly spherical (Fig. 2 [Pl. L8]), although there are small differences between the sloping red and blue wings of the CO $J = 1$–0 absorption profile. A comparison of the absorption-line intensities measured on and off the source-center shows that the wide CO (1–0) absorption feature is spatially extended with respect to the 45″ beam. A similar exercise for the integrated intensity of the central "bump" feature ($-45 < V_{LSR} < 25$ km s^{-1}), measured as an "excess" over the underlying absorption, shows that it is spatially unresolved. In contrast to the CO, an optical *V*-band image taken with the New Technology Telescope (NTT) at ESO (Fig. 2*d*) shows a clearly bipolar morphology.

We have measured a 9 mK upper limit (3 σ) on continuum emission at 89.2 and 145.6 GHz toward the Boomerang Nebula, which is much smaller than the negative temperatures seen in the CO and ^{13}CO $J = 1$–0 spectra, so these must result from absorption of the microwave background, requiring the excitation temperature (T_{ex}) to be less than 2.8 K (T_{bb}). This is because the antenna temperature measured through our "on source–off source" observations is an excess over T_{bb} and is equal to $I(\text{ON}) - I(\text{OFF})$, with $I(\text{ON}) = (\lambda^2/2k)[B(T_{bb})e^{-\tau} + B(T_{ex})(1 - e^{-\tau})]$, and $I(\text{OFF}) = (\lambda^2/2k)B(T_{bb})$, where τ is the optical depth, and B is the Planck blackbody function. Hence, if $T_{ex} < T_{bb}$, and $\tau \gg 1$, then $I(\text{ON}) - I(\text{OFF}) = (\lambda^2/2k)[B(T_{ex}) - B(T_{bb})] < 0$. Using self-consistent modeling of radiative transfer, excitation, and energy balance, Sahai (1990) predicted that if certain conditions were met in the expanding molecular envelopes around late-type stars, then the CO (1–0) excitation temperature, T_{ex}(1–0), could fall below T_{bb} (using certain approximations, Jura, Kahane, & Omont 1988 reached a similar conclusion from an analytic integration of the energy-balance equation).[1] The required conditions are that the mass-loss rate, dM/dt, be high enough to keep the CO (1–0) line optically thick in the outer regions of the envelope, and cooling by adiabatic expansion be sufficient to drive T_{kin}, the gas kinetic temperature, below T_{bb}. The high opacity of the (1–0) line then prevents radiative excitation by the microwave background, and collisional excitation forces T_{ex}(1–0) toward T_{kin}. Under these conditions, little or no absorption occurs in the CO (2–1) line, which usually remains optically thin (since most of the population is in the $J = 0$ level), allowing T_{ex}(2–1) to equalize with T_{bb}.

3. A TWO–SHELL MODEL

We propose a very simple spherically symmetric two-shell model of the Boomerang Nebula that captures the essential physical characteristics of the nebula required to produce the observed CO spectra. The shells are concentric, each characterized by a constant expansion velocity and mass-loss rate (resulting in an inverse-square radial density distribution within each shell). Shell 1 has inner and outer radii $R_{1,i}$ and $R_{1,o}$ of 2.″5 (5.6×10^{16} cm at an assumed source distance of 1500 pc) and 6″ (1.3×10^{17} cm), respectively, and $V_{exp}(1) = 35$ km s^{-1}. Shell 1 is surrounded by shell 2, which has inner radius $= R_{1,o}$ and outer radius $R_2 = 33''$ (7.2×10^{17} cm), and $V_{exp}(2) = 164$ km s^{-1}. In shell 1, $T_{kin} > 2.8$ K, and T_{ex}(1–0) as well as T_{ex}(2–1) are both greater than 2.8 K. In shell 2 ($R_{1,o} < r < R_2$), $T_{kin} < 2.8$ K, T_{ex}(1–0) < 2.8 K, τ(1–0) > 1, T_{ex}(2–1) $= 2.8$ K, and τ(2–1) < 1. The local maximum at the center of the CO and ^{13}CO (1–0) lines is due to emission from shell 1 superposed on absorption due to shell 2. The assumption of sphericity is the simplest one for shell 1, which is unresolved, and reasonable for shell 2, since the contours of absorption intensity shown in Figure 2 show only mild departures from circularity. Radiation from any point in shell 1 can pass unaffected through line-of-sight material in shell 2 because of the Doppler shift induced by the large relative velocities between points in the

[1] However, it was necessary for these authors to assume that the undetermined constant K_0 in their analytic expression for the kinetic temperature $T = K_0 r^{-4/3} + r^{-1}[(\Gamma_0 dM/dT)/(2\pi k\mu V^2)]$ (their eq. [7a]) was sufficiently small in order to reach their conclusion.

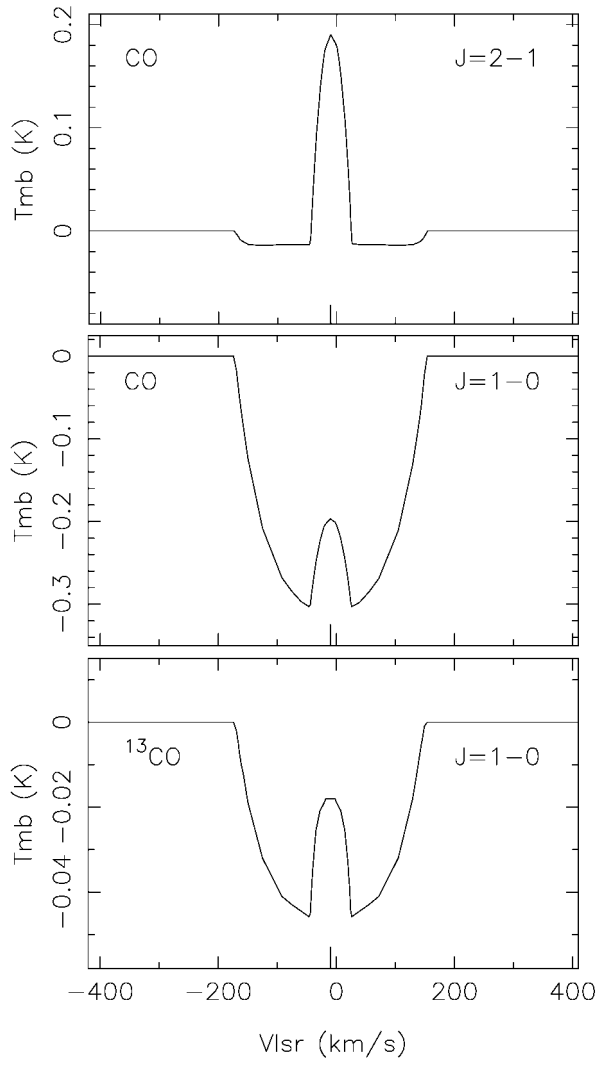

FIG. 3.—Spectra from a two-shell model for the Boomerang Nebula that fit the CO observations reasonably well. The LSR radial velocity of the central star (-10 km s^{-1}) is marked in the spectra. The model consists of two concentric spherical shells, at a distance of 1500 pc, characterized respectively by expansion velocities of 35 and 164 km s^{-1}, outer radii of 1.3×10^{17} and 7.2×10^{17} cm, mass-loss rates of about 10^{-4} and 10^{-3} $M_\odot$ yr^{-1}, and kinetic temperatures greater than 2.8 K and less than 2.8 K.

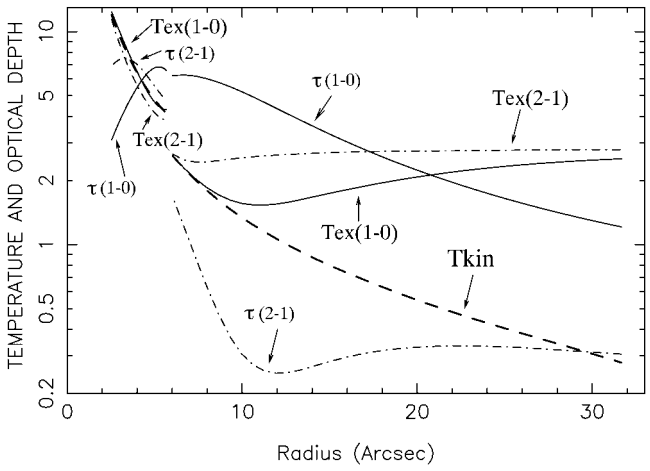

FIG. 4.—CO excitation temperatures and tangential optical depths for the $J = 1$–0 (*solid lines*) and 2–1 (*dot-dashed lines*) transitions from the two-shell model used to fit the observed Boomerang Nebula CO spectra. The kinetic temperature is also shown (*dashed line*). The break in the curves near a radius of 6″ marks the boundary between the inner and outer shells of the model. The excitation temperature of the optically thick $J = 1$–0 line lies below the microwave background temperature (2.8 K) in the outer shell, giving rise to the absorption features in the observed spectra (see Fig. 1).

two shells, simplifying the treatment of radiative transfer. Details of the radiative transfer and statistical equilibrium computation are essentially similar to that for a single spherical shell, as described in Sahai (1987). The model emergent intensity distribution for each transition has been convolved with Gaussian beams of the appropriate sizes to produce spectra that can be directly compared with the observations. The CO/H_2 (number) abundance ratio is found to be about 10^{-3} in the outer shell; the same value has been adopted for the inner shell. Assuming the kinetic temperature to be $T_{\rm kin}(r) = T_0(r/6'')^\beta$, where $\beta = -1.33$, as expected for an envelope where adiabatic cooling dominates all thermodynamic processes, we find $T_0 =$ 4 and 2.8 K in shells 1 and 2. The required mass-loss rates are $\geq 10^{-4}$ $M_\odot$ yr^{-1} in shell 1 and 1.3×10^{-3} $M_\odot$ yr^{-1} in shell 2. Figure 3 shows the model spectra; these fit the data (Fig. 1) reasonably well. Our model also reproduces (to within ~15%) the decrease in CO (1–0) absorption intensity as seen in the mapping data, providing an additional check on the sizes of shells 1 and 2.

The inner radius of shell 1 is sensitively constrained by the ratio of the peak CO (2–1) emission intensity to the amplitude of the central bump in the CO (1–0) spectrum. The kinetic temperature in shell 1 is constrained by the absolute amplitudes of the central bumps in the ^{12}CO and ^{13}CO $J = 1$–0 spectra. The lower absorption and emission intensities of the ^{13}CO data imply that either the size of the ^{13}CO emitting shell is smaller than that of ^{12}CO, or the ^{13}CO emission is optically thin. However, the rounded shapes of the ^{13}CO features imply optical thickness, so the sizes of the ^{13}CO shells must be smaller. A good fit to the ^{13}CO data is obtained with $f(^{13}\text{CO}) = 2.1 \times 10^{-4}$ (assumed same in both shells), inner radii for shells 1 and 2 the same as for CO, but smaller outer radii [3.″9 (8.8×10^{16} cm) and 13″ (2.9×10^{17} cm), respectively]. The latter are smaller than the outer radii of the CO shells because ^{13}CO is photodissociated to a greater extent than CO by interstellar UV (Knapp & Chang 1985) (note that the outer shell cannot shield the inner shell from the UV because of the large Doppler shift induced between the two shells owing to their very different expansion velocities). Models with a significantly lower ^{13}CO abundance are ruled out because they produce absorption-line shapes that are flat-bottomed. The weak absorption seen in the model CO $J = 2$–1 line is well below the noise level in the data. A high signal-to-noise spectrum CO $J = 2$–1 would allow us to constrain the model parameters more precisely. In Figure 4, we show the excitation temperatures and optical depths of the CO $J = 1$–0 and 2–1 lines as a function of radius. The kinetic temperature ($T_{\rm kin}$) in the outer shell must fall rapidly below $T_{\rm bb}$, reaching values as low as (1.0–0.3) K at $r \sim$ (11″–29″), i.e., (2.5–6.5) $\times 10^{17}$ cm, in order to produce the observed absorption features in the CO $J = 1$–0 line.

Further fine tuning of the shell parameters can certainly be done to obtain even better fits. However, such an exercise is not warranted in view of the very simple physical model that we have adopted for the Boomerang Nebula. It is possible that the outflow velocity increases gradually from 35 to 164 km s^{-1} in going from shell 1 to shell 2 across a "transition zone"; however, our data lack sufficient spatial resolution to permit

significant refinements of the radial velocity structure. We now estimate the range of physical parameters that can produce good fits to the data. The derived value of dM/dt ($1.3 \times 10^{-3}\ M_\odot$ yr^{-1}) in shell 2 is very large, even when compared to the highest mass-loss rates seen so far (e.g., using CO spectra, mass-loss rates of about $10^{-4}\ M_\odot$ yr^{-1} have been found in the extended envelopes of CRL 2688 [Truong-Bach et al. 1990] and NGC 7027 [Jaminet et al. 1991]). However, our value of dM/dt is quite robust (uncertain by a factor <1.5), since it is bracketed at the lower end by the requirement that collisional excitation be effective in driving T_{ex}(1–0) sufficiently below 2.8 K [to produce the observed CO (1–0) absorption], and at the upper end by the requirement that the (2–1) optical depth remain smaller than unity (to prevent (2–1) absorption). The CO abundance, f(CO), is constrained by the requirement that f(CO) $\times$ dM/dt must be large enough to make the (1–0) line sufficiently optically thick in shell 2 in order to prevent the microwave background from leaking in and raising T_{ex}(1–0) toward 2.8 K and is about the maximum value expected for a carbon-rich AGB envelope (1.3×10^{-3}, if the O/H abundance is solar and O is fully associated into CO). We have used a source distance of 1500 pc. With $D = 2500$ pc as suggested by BB, even with both f(CO) and dM/dt as high as $10^{-3}\ M_\odot$ yr^{-1}, the CO (1–0) absorption signal is too weak (-0.08 K). Merely increasing the source size does not increase the absorption signal because beyond a certain radius (7×10^{17} cm), the CO (1–0) becomes optically thin, and T_{ex}(1–0) becomes 2.8 K. If $D > 1500$ pc, we require $dM/dt > 10^{-3}\ M_\odot$ yr^{-1} to fit the data. For $D < 1500$ pc, acceptable fits can be obtained by scaling the nebula to keep the angular distribution of kinetic temperature and tangential optical depth the same (requiring dM/dt to scale linearly with D); however, for $D \leq 1000$ pc, the stellar luminosity $L_* \leq 120\ L_\odot$, unacceptably low for the central star of a PPN. The physical properties of shell 1 are more uncertain than those of shell 2. Keeping the CO abundance at the same value as that found for shell 2, the observed amplitudes of the emission bumps in the (2–1) and (1–0) CO spectra require $dM/dt \geq \sim 10^{-4}\ M_\odot$ yr^{-1}. If shell 1 is not spherically symmetric, but confined to an equatorially dense torus-like structure (see § 4), then both the inferred mass-loss rate and temperatures will have to be revised upward.

With the physical parameters of the Boomerang Nebula in hand, we can quantitatively assert that adiabatic cooling dominates the energy balance in shell 2, producing the low kinetic temperatures there. The change of gas temperature with radius in expanding molecular envelopes around late-type stars is governed by $dT/dr = -\frac{4}{3}T/r + [2/(3kVn)][-Q(\text{CO, etc.}) + Q(\text{dust}) + Q(\text{PE}) + Q(\text{CR})]$, where n is the gas number density, V is outflow velocity, Q(CO, etc.) is the cooling rate through millimeter-wave line emission by CO and other molecules, and Q(dust), Q(PE), and Q(CR) are the heating rates respectively due to collisions with dust, photoelectric effect off grains, and cosmic rays (Truong-Bach et al. 1990). The dust heating term is proportional to $(L_*/V)^{0.5} \times$ (dust/gas ratio) $\times$ (mass-loss rate). Thus, the large outflow velocity and relatively low luminosity of the central star in the Boomerang Nebula results in a dust heating rate that is much lower than typical of AGB CSEs. Using $dM/dt = 1.3 \times 10^{-3}\ M_\odot$ yr^{-1}, we find that in shell 2 the adiabatic cooling rate (in units of ergs s^{-1} per H_2 molecule) is 1.4×10^{-25} ($10^{17}/r$ cm), much larger than the rates for dust frictional heating [3×10^{-27} ($10^{17}/r$ cm)^2], cosmic-ray heating (4×10^{-28}), and heating via the photoelectric effect off grains (2.6×10^{-27}).

4. DISCUSSION

The ^{12}C/^{13}C ratio in the Boomerang Nebula is very low (~5), close to the lowest value attainable (3) through equilibrium CNO-cycle nucleosynthesis. Such low values have been observed only in the rare class of J-type carbon stars (e.g., Lambert et al. 1986; Jura et al. 1988). The Boomerang Nebula appears to be a younger counterpart to the young planetary nebula, M1–16, which also has a low ^{12}C/^{13}C ratio, an envelope characterized by a high mass-loss rate, and a relatively low luminosity central star (Sahai et al. 1994). As pointed out by Sahai et al. (1994), for both M1–16 and the Boomerang Nebula, the mechanical wind momentum ($dM/dt \times V_{exp}$) far exceeds the total radiative momentum (L_*/c), making radiation pressure–driven mass-loss mechanisms untenable. Using the luminosity of the Boomerang Nebula central star estimated by BB scaled to our adopted distance of 1500 pc (300 $L_\odot$), the ratio of $dM/dt \times V_{exp}$ to L_*/c comes out to be 4×10^4. The physical mechanism responsible for driving the 164 km s^{-1} outflow in the Boomerang Nebula is thus unknown. The total amount of matter in the Boomerang Nebula is prodigious, with at least 1.9 $M_\odot$ in the outer shell alone, giving a lower limit of about 2.6 $M_\odot$ for the main-sequence progenitor of the Boomerang Nebula (since white dwarf masses lie in a relatively narrow range of 0.5–0.6 $M_\odot$).

The spatiokinematic structure of the Boomerang Nebula (an inner shell with a small expansion velocity and an outer shell with a very large expansion velocity) is unique among AGB/post-AGB objects. If we assume that the expansion velocity of the material in each shell does not change substantially after a short period of initial acceleration, we find that the expansion timescales of the inner and outer shell, 1250 and 1450 yr, respectively, are comparable. We think that it is rather improbable for a single star to produce simultaneously two massive outflows with such different expansion velocities via the same physical mechanism, and we suggest that the inner shell has a different origin than the outer one. A possible mechanism is the ejection of a common envelope (CE) by a central binary star (Livio 1993), with the ejected material being largely confined to low latitudes (i.e., in and near the plane of the nebular waist). The bipolar shape of the optical reflection nebula then results from starlight escaping preferentially from the less dense polar regions of the inner shell and anisotropically illuminating the extended, spherical nebula (i.e., shell 2). This viewpoint is in marked contrast to the traditional one, in which the extended nebula is intrinsically anisotropic, with the density decreasing monotonically with latitude from the equatorial plane (orthogonal to the long axis of the nebula) to the polar axis (Morris 1981). Sahai et al. (1995, 1997) find the traditional model to be untenable in the light of recent high angular resolution optical imaging of the prototype PPN CRL 2688 with the Wide-Field Planetary Camera 2 on the *Hubble Space Telescope* (WFPC2/*HST*).

Our detection of absorption of the microwave background in the CO $J = 1$–0 transition toward the Boomerang Nebula highlights the intimate connection between the kinetic temperature and the mass-loss rate in expanding AGB/post-AGB outflows and raises the troubling possibility that some of the most massive of such outflows remain undetected because the expanding gas has adiabatically cooled down to very low temperatures. It also serves as a telling example of why the estimation of mass-loss rates from CO millimeter-wave line intensities using empirical formulae is fraught with error. A preliminary survey using the SEST to search for CO $J = 1$–0 absorption against the microwave background in several other

post–AGB objects (Hen 401, He 2–113, HD 44179, and M1–16) has so far yielded only null results. Further studies of the Boomerang Nebula are underway, including *R*-band polarimetric imaging observations with WFPC2/*HST*.

We thank Roland Gredel for obtaining the ESO NTT image. The Swedish ESO Submillimetre Telescope (SEST) is operated jointly by ESO and the Swedish National Facility for Radioastronomy, Onsala Space Observatory at Chalmers University of Technology. R. S. is grateful for partial support from the National Research Council (National Academy of Sciences) and NASA grant NAS7-1260.

REFERENCES

Bujarrabal, V., & Bachiller, R. 1991, A&A, 242, 247 (BB)
Jaminet, P. A., Danchi, W. C., Sutton, E. C., Russell, A. P. G., Sandell, G., Bieging, J. H., & Wilner, D. A. 1991, ApJ, 380, 461
Jura, M., Kahane, C., & Omont, A. 1988, A&A, 201, 80
Knapp, G. R., & Chang, K. M. 1985, ApJ, 293, 281
Lambert, D. L., Gustafsson, B., Eriksson, K., & Hinkle, K. H. 1986, ApJS, 62, 373
Latter, W. B., Hora, J. L., Kelly, D. M., Deutsch, L. K., & Maloney, P. R. 1993, AJ, 106, 260
Livio, M. 1993, in IAU Symp. 155, Planetary Nebulae, ed. R. Weinberger & A. Acker (Dordrecht: Kluwer), 279
Morris, M. 1981, ApJ, 249, 572
Neckel, T., Staude, H. J., Sarcander, M., & Birkle, K. 1987, A&A, 175, 231
Sahai, R. 1987, ApJ, 318, 809
———. 1990, ApJ, 362, 652
Sahai, R., et al. 1995, BAAS, 27, 1344
———. 1997, ApJ, in press
Sahai, R., Wootten, A., Schwarz, H. E., & Wild, W. 1994, ApJ, 428, 237
Schwarz, H. E., Corradi, R. L. M., & Melnick, J. 1992, A&AS, 96, 23
Schönberner, D. 1990, in From Miras to Planetary Nebulae: Which Path for Stellar Evolution? ed. M. O. Mennessier & A. Omont (Gif-sur-Yvette: Editions Frontières), 355
Taylor, K. N. R., & Scarrot, S. M. 1980, MNRAS, 193, 321
Truong-Bach, Morris, D., Nguyen-Q-Rieu, & Deguchi, S. 1990, A&A, 230, 431
Wegner, G., & Glass, I. S. 1979, MNRAS, 188, 327

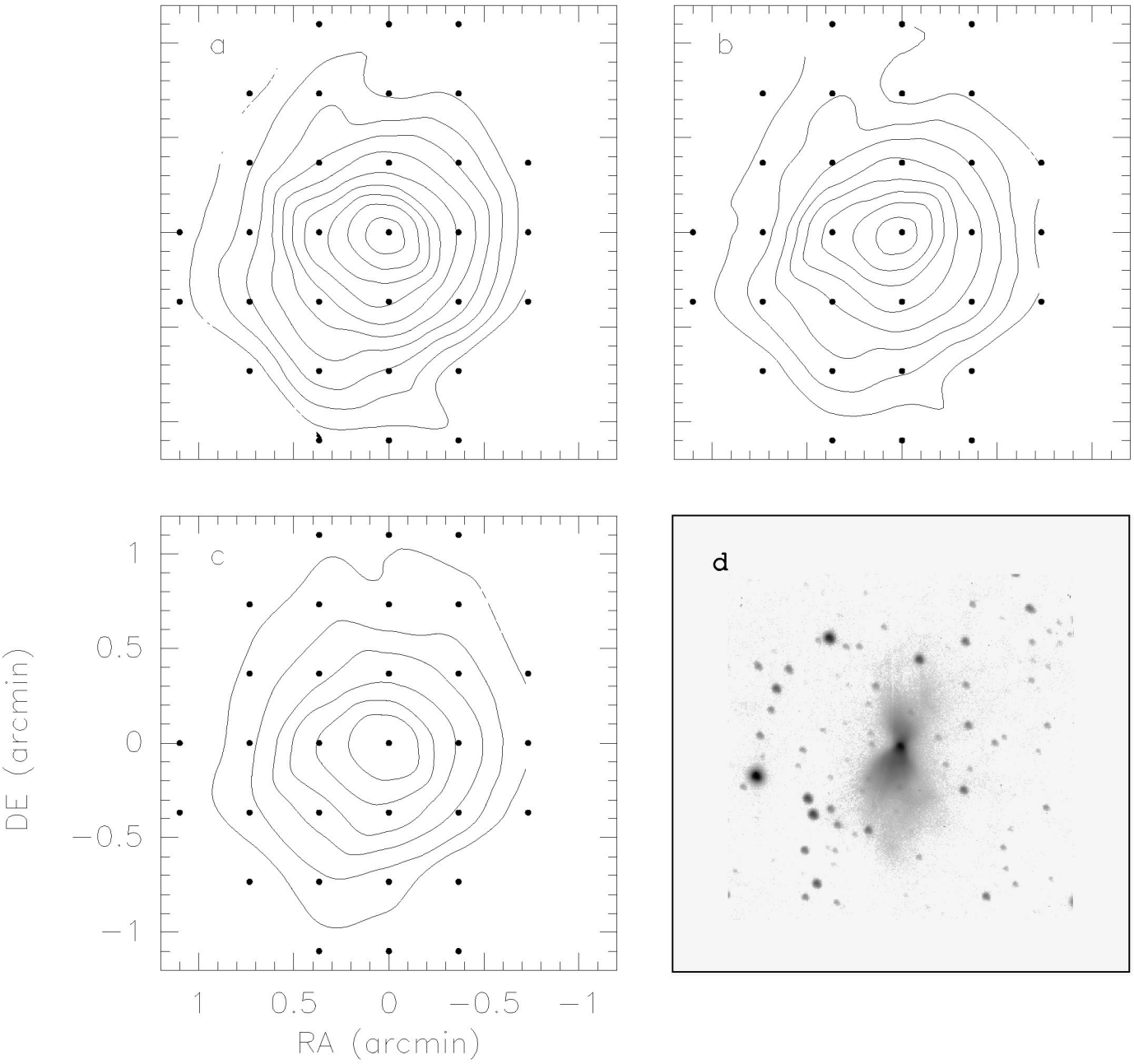

FIG. 2.—Contour maps of the CO (1–0) features in different velocity intervals, and an optical image taken with the NTT at ESO. The CO data were taken every 22″, half the telescope beamwidth. Dots mark observed positions. The spatial scale, shown only in (*c*), is the same for all panels. (*a*) The intensity integrated over the full velocity extent of the CO feature (−180 to 156 km s^{-1}). Contours are from −40 to −4 in steps of 4 K km s^{-1}. (*b*, *c*) The intensity integrated over velocity subintervals in the blue (−180 to −43 km s^{-1}) and red wings (23 to 156 km s^{-1}) of the feature, showing regions of the high-velocity outflow moving toward (*b*) and away from us (*c*). Contours are in steps of −2 K km s^{-1} starting at −2 K km s^{-1}. The 1 σ noise in the CO maps is about 0.7 K km s^{-1}. (*d*) A logarithmically stretched, uncalibrated optical *V*-band image in inverted gray scale (with the same spatial scale as the CO maps). Since the CO maps show only small departures from circular symmetry, we assume a spherical distribution of molecular gas in the nebula for modeling purposes.

SAHAI & NYMAN (see 487, L156)